

Non-Hermitian skin effect of dislocations and its topological origin


Balaganchi A. Bhargava,¹ Ion Cosma Fulga,¹ Jeroen van den Brink,^{1,2} and Ali G. Moghaddam^{3,4,1}

¹*Institute for Theoretical Solid State Physics, IFW Dresden and Würzburg-Dresden Cluster of Excellence ct.qmat, Helmholtzstrasse 20, D-01069 Dresden, Germany*

²*Institute for Theoretical Physics, TU Dresden, D-01069 Dresden, Germany*

³*Department of Physics, Institute for Advanced Studies in Basic Sciences (IASBS), Zanjan 45137-66731, Iran*

⁴*Computational Physics Laboratory, Physics Unit, Faculty of Engineering and Natural Sciences, Tampere University, P.O. Box 692, FI-33014 Tampere, Finland*

 (Received 8 June 2021; revised 22 November 2021; accepted 29 November 2021; published 8 December 2021)

We demonstrate that dislocations in two-dimensional non-Hermitian systems can give rise to density accumulation or depletion through the localization of an extensive number of states. These effects are shown by numerical simulations in a prototype lattice model and expose a different face of the non-Hermitian skin effect, by disentangling it from the need for boundaries. We identify a topological invariant responsible for the dislocation skin effect, which takes the form of a \mathbb{Z}_2 Hopf index that depends on the Burgers vector characterizing the dislocations. Remarkably, we find that this effect and its corresponding signature for defects in Hermitian systems fall outside of the known topological classification based on bulk-defect correspondence.

DOI: [10.1103/PhysRevB.104.L241402](https://doi.org/10.1103/PhysRevB.104.L241402)

Introduction. The Hermiticity of observables in quantum mechanics is a concrete part of their mathematical structure and physical interpretations. However, upon dealing with dissipative quantum systems as well as a variety of classical platforms such as electrical circuits, photonic crystals, and mechanical metamaterials, non-Hermitian (NH) Hamiltonians can effectively describe an essential part of their dynamics [1–5]. Recently, in light of overwhelming interest and progress in understanding topological phases, NH models have been also revisited from a topological point of view [6,7]. Although they share certain similarities with Hermitian systems, NH systems possessing complex energy spectra can reveal quite distinct topological features [8,9]. In particular, it has been found that in absolute contrast to any Hermitian system, in NH models the presence of open boundaries can drastically affect the energy spectra, and subsequently all eigenstates accumulate towards one end of the system, a phenomenon called the non-Hermitian skin effect (NHSE) [10–28]. This effect, which necessitated revisiting the concept of bulk-boundary correspondence in Hermitian topological phases [29–32], originates from nontrivial point gap topology, represented by the one-dimensional (1D) winding number of the complex energy bands [33,34].

Here, we address the question of how the NHSE manifests in the presence of topological defects such as dislocations, instead of open boundaries. Many studies have revealed the presence of topologically protected modes at defects in Hermitian topological systems [35–45]. The topological defects have been thoroughly classified by Teo and Kane, who have put forward the concept of bulk-defect correspondence [46–48]. The classification of topological defects has been also extended to NH systems [49], and very recent works have examined defect modes in NH topological phases [50–52].

However, the interplay between nontrivial defects and point gap topology, the latter being an intrinsically NH feature, still remains to be understood.

By considering a prototype two-dimensional (2D) NH lattice model, we find both a macroscopically large density accumulation and also density depletion in the vicinity of dislocations, which we respectively call skin and antiskin effects (see Fig. 1). This observation not only shows an unexplored consequence of the NHSE effect, but strikingly it is related to a Hermitian topological system hosting a different type of bulk-defect correspondence, beyond the known *stable* classifications [46,47]. Nevertheless, we identify a topological invariant $\vartheta = \hat{\mathbf{z}} \cdot (\mathbf{v} \times \mathbf{B})/2$ to diagnose the macroscopic density collapse in terms of the Burgers vector \mathbf{B} of the dislocation and two weak indices, $\mathbf{v} = (v_x, v_y)$, which are the 2D averaged winding numbers. We show that the topological invariant ϑ has an integer/half-integer parity given by the topological θ term. We further provide an intuitive picture for ϑ in connection with topological invariants of weak topological phases of Hermitian systems subjected to topological defects.

Weak Hatano-Nelson model. As a preliminary, we first consider the simplest prototypical model which shows the NHSE, the Hatano-Nelson (HN) model described by the Hamiltonian $\mathcal{H}_{\text{IDHN}} = \sum_{j,\eta=\pm 1} (t + \eta \delta t) c_{j+\eta}^\dagger c_j$ as a single-orbital tight-binding chain with nonreciprocal hoppings [53,54]. A nonzero winding number of energy bands given by

$$\nu = \frac{1}{2\pi i} \int_{-\pi}^{\pi} dk \frac{\partial \varepsilon(k)}{\partial k} \frac{1}{\varepsilon(k)} = \text{sgn}(\delta t) = \pm 1 \quad (1)$$

signals the existence of the NHSE, revealed by the sensitivity of all eigenstates to the boundary conditions and the breakdown of the conventional bulk-boundary correspondence. The

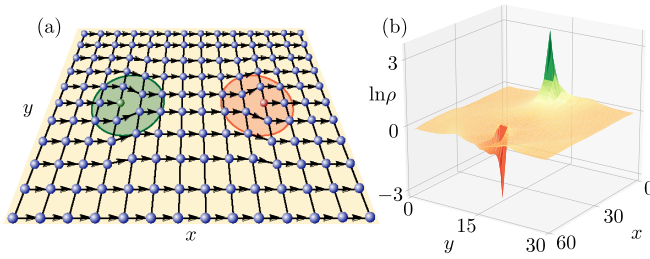


FIG. 1. (a) Sketch of the WHN model with two dislocations which are indicated by encircling them. (b) Logarithm of local density profile of the system with $L = 30$ and under periodic boundary conditions and using a logarithmic scale for the density. The green peak and red dip represent the skin and antiskin effects in which an extensive number of exponentially localized states are piled up and depleted from the two dislocations, respectively.

NHSE can be characterized in terms of the localization of the probability density defined as $\rho_{\mathbf{r}} = \sum_n |\langle \mathbf{r} | \psi_n^R \rangle|^2$ in which $|\psi_n^R\rangle$ is the n th right eigenstate of the Hamiltonian, $|\mathbf{r}\rangle$ is the position ket, and the summation is over all eigenstates regardless of eigenvalue. For a 1D HN model with open boundaries, all eigenstates are localized towards one end, and as a consequence, the probability density is $\rho_r \propto e^{r/\xi_{1D}}$ with a 1D localization length $\xi_{1D} = 1/\log[(t + \delta t)/(t - \delta t)]$ determined by the strength of nonreciprocity δt .

We construct a 2D model by stacking HN chains along the y direction, with nearest-neighbor interchain hoppings as schematically shown in Fig. 1(a), and with the Hamiltonian

$$\mathcal{H} = \sum_{\mathbf{r}} \sum_{\eta=\pm 1} [(t_x + \eta \delta t_x) c_{\mathbf{r}+\eta\hat{x}}^\dagger c_{\mathbf{r}} + t_y c_{\mathbf{r}+\eta\hat{y}}^\dagger c_{\mathbf{r}}], \quad (2)$$

in which only hoppings in the x direction are nonreciprocal [55]. We refer to this Hamiltonian as the *weak* HN model (WHN), in analogy to weak topological insulators which are formed by stacking lower-dimensional strong topological insulators. Its eigenvalues form a family of ellipses in the complex plane which wind around the origin as a function of momentum $\varepsilon_{\mathbf{k}} = 2(t_x \cos k_x + t_y \cos k_y + i \delta t_x \sin k_x)$. In momentum space, the Hamiltonian $\mathcal{H}_{\mathbf{k}}$ corresponding to Eq. (2) can be considered as a stack of decoupled 1D HN models with a k_y -dependent chemical potential $2t_y \cos k_y$. We introduce weak indices

$$\nu_j = \int \frac{d^2\mathbf{k}}{i(2\pi)^2} \mathcal{H}_{\mathbf{k}}^{-1} \partial_{k_j} \mathcal{H}_{\mathbf{k}}, \quad (3)$$

as the average of two 1D winding number densities $\nu(k_j)$ along the $j = x, y$ directions. As long as $|t_y| < |t_x|$, there exists a point gap at $\varepsilon = 0$ in the spectrum. Subsequently, the weak indices Eq. (3) are quantized, and for our particular stacked model we obtain $\nu_x = \text{sgn}(\delta t_x)$ and $\nu_y = 0$. Consequently, for a system with open boundaries all states show a NHSE along the x direction and, depending on the sign of δt_x , they localize either on the left or the right edge.

Dislocation-induced skin effect. We consider a rectangular system consisting of $2L \times L$ sites in the x and y directions, imposing periodic boundary conditions (PBCs) in order to form a torus and introduce two dislocations separated by a length of L sites using the cut and glue procedure. A row of

L sites is first removed from the system, and the resulting cut is glued back together using vertical hoppings t_y , as shown in Fig. 1(a).

We find that the density localizes at one of the dislocations, forming a peak, and depletes at the other one, forming a dip [see Fig. 1(b), obtained for $t_y/t_x = 0.4$, $\delta t_x/t_x = 0.6$]. This behavior is indeed different from the conventional NHSE, although the underlying mechanisms are the nonreciprocity of the hopping parameters in both cases. First, the localized density depletion around the second dislocation (antiskin effect) is a feature of the NHSE which does not occur in uniform, defect-free NH systems. Second, in spite of the fact that vertical hopping terms are reciprocal, the exponential accumulation and depletion of the density around the dislocations take place in both the x and the y directions, as can be seen in Fig. 1(b).

The formation of skin and antiskin effects at the dislocations can be understood intuitively in two different ways. The first is to consider the decoupled limit, $t_y = 0$, in which the system consists of independent 1D Hatano-Nelson models. In this case, introducing dislocations amounts to removing half of the sites from one of the HN chains, such that it goes from periodic to open boundary conditions. This leads to the formation of a NHSE at its boundaries [red and green sites in Fig. 1(a)]. However, the skin and antiskin effects are present also when $t_y \neq 0$. This fact can be understood as arising from the nonreciprocal hoppings in the horizontal direction. For $\delta t_x > 0$, the hopping to the right is larger than the hopping to the left, implying that states will be pumped in the direction of the larger hopping [56], as indicated by arrows in Fig. 1(a). Examining a closed loop surrounding each of the two dislocations, shown by green and red circles, we find that the number of arrows pointing into the contour is different from the number pointing out of the contour. This imbalance is consistent with the density accumulation and depletion shown in Fig. 1(b), suggesting that states are pumped into or out of the dislocations cores.

Scaling properties. In order to show the extensive nature of the NHSE caused by the dislocation, we study numerically the length dependence of the maximum of the density in the vicinity of one dislocation. For a 1D HN model, the maximum density is easily obtained from its conservation law $\int dr \rho_r = L$ which leads to $\rho_{\max} = (L/\xi)/(1 - e^{-L/\xi}) \approx L/\xi$. We find that also in the 2D case, the linear behavior of the maximum density persists [see Fig. 2(a)], and our results are consistent with $\rho_{\max} \propto L$ for a wide range of parameter values t_y/t_x and $\delta t_x/t_x$. When keeping the system size constant, we observe that the maximum density is larger when $t_y \neq 0$ compared to the decoupled limit. This indicates that the dislocation-induced NHSE is different from that occurring in the 1D model, in the sense that states from the entire 2D system participate in the density collapse.

In contrast to the scaling behavior of the skin effect, the antiskin effect saturates as a function of system size, with the minimum density ρ_{\min} becoming independent of L for large systems. The precise values of ρ_{\min} depend both on nonreciprocity as well as the strength of the vertical hoppings, but they are usually a few orders of magnitude smaller than the density far away from the dislocations, as can be seen also in Fig. 1(b).

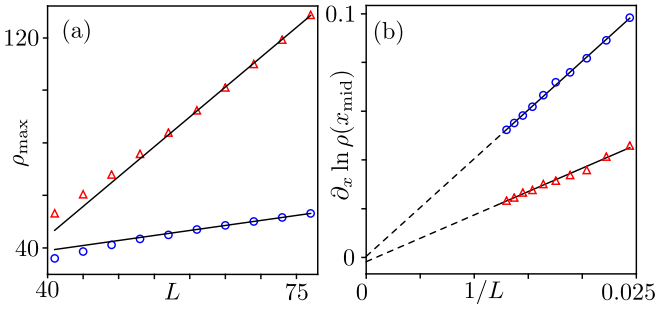


FIG. 2. (a) Maximum density plotted as a function of system size L for two values of $(\delta t_x/t_x, t_y/t_x) = (0.9, 0.04)$, shown using blue circles, and $(0.72, 0.72)$, shown as red triangles. For large systems, $\rho_{\max} \propto L$, as indicated by the black lines. (b) Slope of the density $\partial(\ln \rho_{\text{mid}})/\partial x$ for the same parameters. The slope is averaged over five neighboring lattice sites at the midpoint of the line connecting the dislocations. In the thermodynamic limit, the fit indicates a vanishing slope (within error bars), as shown by the black lines.

Finally, we study the behavior of the density far from the cores of the dislocations. We find that the density is roughly uniform as a function of the coordinates x and y , with the largest variations occurring on a line connecting the two dislocations, corresponding to the 1D chain left over after removing L sites from the system (the row of sites terminating at the dislocations in Fig. 1). We examine the length dependence of the slope of the density at the midpoint of this chain, $\partial_x \ln \rho(x_{\text{mid}})$. When extrapolating to $L \rightarrow \infty$ for different t_y/t_x and $\delta t_x/t_x$, we observe that the slope vanishes, indicating that in the thermodynamic limit the density profile is flat far away from the dislocation cores [see Fig. 2(b)]. This is in contrast to the density profile of the 1D Hatano-Nelson model, where $\rho_r \propto e^{r/\xi_{\text{1D}}}$ implies a nonzero $\partial_r \ln \rho(r_{\text{mid}}) \sim 1/\xi_{\text{1D}}$, independent of system size. The uniform density far from the dislocation cores is similar to the behavior of Hermitian systems hosting topological defects, where the defect is locally indistinguishable sufficiently far away from its core. Here, however, $O(L)$ states accumulate at one of the dislocations, and the remaining $O(L^2 - L)$ appear to be distributed uniformly away from the defect cores.

Topological origin. To determine the topological invariant associated with the dislocation-induced skin and antiskin effects, we use the procedure outlined in Refs. [33,57]. Starting from our NH system, we construct a doubled Hermitian Hamiltonian with chiral symmetry as

$$\tilde{\mathcal{H}} = \begin{pmatrix} 0 & \mathcal{H} \\ \mathcal{H}^\dagger & 0 \end{pmatrix}. \quad (4)$$

As shown in Ref. [33], the topological invariant responsible for the NHSE in \mathcal{H} is identical to the one responsible for the existence of topologically protected midgap states in $\tilde{\mathcal{H}}$.

The doubled system is a stack of horizontal Su-Schrieffer-Heeger (SSH) chains [58], coupled by diagonal hoppings. It belongs to the class BDI in the Altland-Zirnbauer classification [59], and has been discussed in Ref. [60]. Using the Hermitian model Eq. (4), we find that the bulk of the system is gapped provided that $|t_y| < |t_x|$, and that each of the two dislocations traps an exponentially localized zero-energy mode. These midgap modes are protected by chiral symmetry,

which forces the spectrum to be symmetric around $E = 0$. As a consequence, the energy of the dislocation-bound states cannot be shifted away from zero unless the bulk gap closes, or the two defects are brought in proximity of each other, such that their bound states can hybridize and gap out.

The doubled model provides a convenient starting point to demonstrate the topological origin of the NHSE caused by the dislocations. In Hermitian systems, it has been shown that protected midgap states can appear not only at the boundaries but can be also trapped by topological defects. In the latter case, their existence relies on the topological properties of defect Hamiltonians $\mathcal{H}(\mathbf{k}, \mathbf{r})$, with \mathbf{r} spanning a D -dimensional sphere around the defect, as proposed by Teo and Kane [46]. At each point \mathbf{r} far away from the defect, $\mathcal{H}(\mathbf{k}, \mathbf{r})$ is well approximated by a Bloch Hamiltonian since the lattice is locally translation symmetric. However, upon encircling around the dislocation as indicated in Fig. 1(a), an extra translation by the Burgers vector \mathbf{B} is needed as compared to a similar loop in the absence of the dislocation.

For our 2D model in the presence of a dislocation we can devise a NH defect Hamiltonian $\mathcal{H}(\mathbf{k}, s)$ with 2D momenta \mathbf{k} and a variable $s \in [0, 1]$ which describes the loop around the topological defect. The doubled Hamiltonian $\tilde{\mathcal{H}}(\mathbf{k}, s)$ corresponds to a 2D chiral-symmetric system with a point defect, which is characterized by the 3D winding number,

$$W_3 = \frac{\epsilon^{\mu\nu\lambda}}{3} \int \frac{d^2 \mathbf{k} ds}{(2\pi i)^3} \text{Tr}(q \partial_\mu q^\dagger q \partial_\nu q^\dagger q \partial_\lambda q^\dagger), \quad (5)$$

according to the topological classification of Ref. [46]. The integration is over $T^2 \times S^1$ (the effective 3D Brillouin zone of the defect Hamiltonian), $\epsilon^{\mu\nu\lambda}$ is the fully antisymmetric Levi-Civita tensor, and $q(\mathbf{k}, s) = \mathcal{H}/(\mathcal{H}\mathcal{H}^\dagger)^{1/2}$ results after flattening the bands of the Hermitian Hamiltonian $\tilde{\mathcal{H}}(\mathbf{k}, s)$. Since our WHN model has only one band, $q(\mathbf{k}, s)$ is a scalar, which means that the winding number in Eq. (5) vanishes identically (due to the Levi-Civita tensor). This means that W_3 fails to capture the existence of topological zero modes of the doubled defect Hamiltonian $\tilde{\mathcal{H}}$, and thus also fails to capture the dislocation-induced NHSE.

This motivates us to formulate an alternative approach, where instead of working with the defect Hamiltonian, we displace locally the Bloch wave functions as $u_{\mathbf{k},s}(\mathbf{r}) = u_{\mathbf{k}}^0(\mathbf{r} - s\mathbf{B})$ along the loop surrounding the dislocation, where $u_{\mathbf{k}}^0$ denotes the Bloch state of the defect-free crystal. That way the interplay of the defected lattice represented by the Burgers vector and band-structure topology are directly introduced through the displaced Bloch wave functions. Consequently, the Berry connection of the system in the presence of a topological defect reads

$$\mathbf{A}(\mathbf{k}, s) = \langle u_{\mathbf{k},s} | \nabla_{\mathbf{k},s} | u_{\mathbf{k},s} \rangle = \mathbf{A}^0(\mathbf{k}) + \hat{\mathbf{z}} A_s(\mathbf{k}), \quad (6)$$

consisting of a defect-free part $\mathbf{A}^0(\mathbf{k}) = \langle u_{\mathbf{k},s}^0 | \nabla_{\mathbf{k}} | u_{\mathbf{k},s}^0 \rangle$ and an additional term due to the defects. We find that the defect-free part is given by $\mathbf{A}^0(\mathbf{k}) = \frac{1}{2} q_{\mathbf{k}}^{-1} \nabla_{\mathbf{k}} q_{\mathbf{k}}$ with $q_{\mathbf{k}} = \epsilon_{\mathbf{k}}/|\epsilon_{\mathbf{k}}|$, since the Bloch states for the doubled Hamiltonian are given by $|u_{\mathbf{k}}^0\rangle = (1/\sqrt{2})(q_{\mathbf{k}}, 1)^T$. The defect-enforced term $A_s(\mathbf{k}) = \langle u_{\mathbf{k},s} | \partial_s | u_{\mathbf{k},s} \rangle$ in Eq. (6), which originates from displacing Bloch states by the fictitious momentum s , can be written as

[46,61]

$$A_s(\mathbf{k}) = -\mathbf{B} \cdot \langle u_{\mathbf{k}}^0 | \nabla_{\mathbf{r}} | u_{\mathbf{k}}^0 \rangle = i \mathbf{B} \cdot \mathbf{k} - \mathbf{B} \cdot \mathbf{a}^p(\mathbf{k}), \quad (7)$$

where $\mathbf{a}^p(\mathbf{k}) = \langle u_{\mathbf{k}}^0 | (\nabla_{\mathbf{r}} + i\mathbf{k}) | u_{\mathbf{k}}^0 \rangle$ is periodic over the reciprocal space [62]. Now, associated with the Berry connection (6), there exist a Chern-Simons (CS) form $\mathcal{Q}_3(\mathbf{k}, s) = d^2\mathbf{k}ds \epsilon^{\mu\nu\lambda} \text{Tr}(A_\mu \partial_\nu A_\lambda + \frac{2}{3}A_\mu A_\nu A_\lambda)$. From a detailed derivation [61], we find a \mathbb{Z}_2 , CS invariant,

$$\vartheta = \frac{1}{(2\pi)^2} \int_{T^2 \times S^1} \mathcal{Q}_3 = \frac{1}{2} \hat{\mathbf{z}} \cdot (\mathbf{B} \times \mathbf{v}) \pmod{1}, \quad (8)$$

determined by the cross product of the Burgers vector, and the 2D weak indices of the WHN model, Eq. (3). The \mathbb{Z}_2 invariant $\vartheta \in \{0, 1/2\}$ can distinguish between the trivial and nontrivial phases of the doubled Hamiltonian in the presence of topological defects. $\vartheta = 1/2$ implies an odd parity of zero modes at a dislocation in the doubled Hamiltonian, and consequently the skin effect of topological defects in the WHN model. The two dislocations shown in Fig. 1 are characterized by Burgers vectors $\mathbf{B} = (B_x, B_y) = (0, \pm 1)$, which, together with weak indices $\mathbf{v} = (1, 0)$ for $\delta t_x > 0$, imply a half integer ϑ . Remarkably, both the skin *and* antiskin effects are associated with a nontrivial invariant, signaling that also the localized density depletion around one of the dislocations is topological in origin.

The topological invariant Eq. (8) is reminiscent of that characterizing dislocations in Hermitian weak topological phases [46]. The invariant there also involves both the Burgers vector and the vector of weak indices, though their scalar product instead of the cross product. As in that case, an intuitive understanding can be gained by going to the decoupled limit, where the Burgers vector specifies which type of termination is introduced into one of the chains, and the weak invariants control which terminations will show the NHSE. Furthermore, due to the correspondence, unraveled in Ref. [33], between the NHSE and the topology of Hermitian systems given by Eq. (4), the invariant ϑ can be equally used for the 2D Hermitian model. Namely, we can use it to predict the appearance of zero modes bounded to dislocations in a 2D model consisting of arrays of SSH chains.

We emphasize that the CS invariants are not gauge invariant in general, hence, ϑ only captures the integer/half-integer parity of the $\mathbb{Z}/2$ invariant $\hat{\mathbf{z}} \cdot (\mathbf{B} \times \mathbf{v})/2$. As such, it can only distinguish the even or odd parity of dislocation-bound zero modes of the doubled, Hermitian model $\tilde{\mathcal{H}}$, and not their total number. This can be better understood by noting that for a single-band 2D NH model, the Berry connection $\mathbf{A}(\mathbf{k}, s)$ is a 3D Abelian gauge field, and consequently the CS invariant ϑ is identical to the *Hopf index* [63–66]. The Hopf index is generally a $\mathbb{Z}_{2N_{\text{Ch}}}$ invariant where the integer $N_{\text{Ch}} = \text{GCD}(C_x, C_y, C_s)$ is the greatest common divisor of three Chern numbers $C_j = \int d^2k_\perp \Omega_j$ defined over three 2D cross sections of $T^2 \times S^1$. Using the definition of Berry curvature $\Omega_j = \epsilon_{jkl} \partial_k A_l$ and the Berry connection given by Eq. (6), we find $(C_x, C_y, C_s) = (B_y, -B_x, 0)$ with $\text{GCD} = 1$,

which justifies the \mathbb{Z}_2 nature of the topological invariant ϑ [61]. The correspondence between the WHN model with topological defects and Hopf insulators indicates that it also lies in the nonstable regime (the numbers of energy bands are below the bounds introduced in Ref. [67]). As a result, it falls beyond the periodic table of stable phases where 2D chiral-symmetric systems with point defects are characterized with the winding number $W_3 \in \mathbb{Z}$ [46].

Finally, we find that, consistent with the topological invariant of Eq. (8), the density peak and dip shown in Fig. 1 lose their robustness when $\mathbf{B} \times \mathbf{v} = \mathbf{0}$, or when the point gap at $\varepsilon = 0$ closes ($|t_y| \geq |t_x|$). We explore these cases in the Supplemental Material [61], comparing the nontrivial point defects studied above with trivial point defects, such as vacancies. We find that, while localized features in the density are still observed, for trivial point defects they are much weaker, and can be suppressed by means of local perturbations. They are similar to the conventional impurity states present in Hermitian systems, which do cause localized features in the local density of states, but do not show the robustness associated with the nontrivial topology.

Conclusions. Using a prototypical 2D non-Hermitian system, we have shown that dislocations result in the formation of a non-Hermitian skin effect, signaled by the accumulation of density due to the localization of a macroscopically large number of states towards the dislocation. This effect is observed numerically, and then understood using a topological invariant that falls outside the conventional, stable bulk-defect correspondence. The analytical study of this density accumulation as well as its extensions to arrays of dislocations provides an interesting avenue for further research.

Unlike the skin effect associated with the boundaries of non-Hermitian systems, we have found that dislocations can also host the antiskin effect. This is a topologically protected *depletion* of an otherwise uniform density profile, which occurs at the dislocation core. The possibility of an antiskin effect offers an additional tool for tailoring the positions of eigenstates in non-Hermitian systems, and may be useful in the design of practical applications, such as sensors [68] or light funnels [19].

Note added in proof. Recently, we became aware of Ref. [52], in which the authors observe the presence of skin effects at dislocations in NH systems, including for a model that is equivalent to our WHN system.

Acknowledgments. We thank C. L. Kane and A. R. Akhmerov for enlightening discussions, as well as Ulrike Nitzsche for technical assistance. This work was supported by the Deutsche Forschungsgemeinschaft (DFG, German Research Foundation) under Germany's Excellence Strategy through the Würzburg-Dresden Cluster of Excellence on Complexity and Topology in Quantum Matter – *ct.qmat* (EXC 2147, project-id 390858490), as well as through the DFG grant FU 1253/1-1. A.G.M. acknowledges financial support from Iran Science Elites Federation under Grant No. 11/66332.

- [1] C. M. Bender, Making sense of non-Hermitian Hamiltonians, *Rep. Prog. Phys.* **70**, 947 (2007).
- [2] I. Rotter, A non-Hermitian Hamilton operator and the physics of open quantum systems, *J. Phys. A: Math. Theor.* **42**, 153001 (2009).
- [3] R. El-Ganainy, K. G. Makris, M. Khajavikhan, Z. H. Musslimani, S. Rotter, and D. N. Christodoulides, Non-Hermitian physics and PT symmetry, *Nat. Phys.* **14**, 11 (2018).
- [4] T. Ozawa, H. M. Price, A. Amo, N. Goldman, M. Hafezi, L. Lu, M. C. Rechtsman, D. Schuster, J. Simon, O. Zilberberg, and I. Carusotto, Topological photonics, *Rev. Mod. Phys.* **91**, 015006 (2019).
- [5] Y. Ashida, Z. Gong, and M. Ueda, Non-Hermitian physics, *Adv. Phys.* **69**, 249 (2020).
- [6] Z. Gong, Y. Ashida, K. Kawabata, K. Takasan, S. Higashikawa, and M. Ueda, Topological Phases of Non-Hermitian Systems, *Phys. Rev. X* **8**, 031079 (2018).
- [7] V. M. Alvarez, J. B. Vargas, M. Berdakin, and L. F. Torres, Topological states of non-Hermitian systems, *Eur. Phys. J. Spec. Top.* **227**, 1295 (2018).
- [8] E. J. Bergholtz, J. C. Budich, and F. K. Kunst, Exceptional topology of non-Hermitian systems, *Rev. Mod. Phys.* **93**, 015005 (2021).
- [9] K. Kawabata, K. Shiozaki, M. Ueda, and M. Sato, Symmetry and Topology in Non-Hermitian Physics, *Phys. Rev. X* **9**, 041015 (2019).
- [10] T. E. Lee, Anomalous Edge State in a Non-Hermitian Lattice, *Phys. Rev. Lett.* **116**, 133903 (2016).
- [11] S. Yao and Z. Wang, Edge States and Topological Invariants of Non-Hermitian Systems, *Phys. Rev. Lett.* **121**, 086803 (2018).
- [12] V. M. Martinez Alvarez, J. E. Barrios Vargas, and L. E. F. Foa Torres, Non-Hermitian robust edge states in one dimension: Anomalous localization and eigenspace condensation at exceptional points, *Phys. Rev. B* **97**, 121401(R) (2018).
- [13] C. H. Lee and R. Thomale, Anatomy of skin modes and topology in non-Hermitian systems, *Phys. Rev. B* **99**, 201103(R) (2019).
- [14] F. Song, S. Yao, and Z. Wang, Non-Hermitian Skin Effect and Chiral Damping in Open Quantum Systems, *Phys. Rev. Lett.* **123**, 170401 (2019).
- [15] T. Helbig, T. Hofmann, S. Imhof, M. Abdelghany, T. Kiessling, L. Molenkamp, C. Lee, A. Szameit, M. Greiter, and R. Thomale, Generalized bulk–boundary correspondence in non-Hermitian topoelectrical circuits, *Nat. Phys.* **16**, 747 (2020).
- [16] S. Longhi, Probing non-Hermitian skin effect and non-Bloch phase transitions, *Phys. Rev. Res.* **1**, 023013 (2019).
- [17] F. Song, S. Yao, and Z. Wang, Non-Hermitian Topological Invariants in Real Space, *Phys. Rev. Lett.* **123**, 246801 (2019).
- [18] L. Xiao, T. Deng, K. Wang, G. Zhu, Z. Wang, W. Yi, and P. Xue, Non-Hermitian bulk–boundary correspondence in quantum dynamics, *Nat. Phys.* **16**, 761 (2020).
- [19] S. Weidemann, M. Kremer, T. Helbig, T. Hofmann, A. Stegmaier, M. Greiter, R. Thomale, and A. Szameit, Topological funneling of light, *Science* **368**, 311 (2020).
- [20] T. Hofmann, T. Helbig, F. Schindler, N. Salgo, M. Brzezińska, M. Greiter, T. Kiessling, D. Wolf, A. Vollhardt, A. Kabaši, C. H. Lee, A. Bilušić, R. Thomale, and T. Neupert, Reciprocal skin effect and its realization in a topoelectrical circuit, *Phys. Rev. Res.* **2**, 023265 (2020).
- [21] J. Claes and T. L. Hughes, Skin effect and winding number in disordered non-Hermitian systems, *Phys. Rev. B* **103**, L140201 (2021).
- [22] Y. Ma and T. L. Hughes, The quantum skin Hall effect, [arXiv:2008.02284](https://arxiv.org/abs/2008.02284).
- [23] L. Li, C. H. Lee, S. Mu, and J. Gong, Critical non-Hermitian skin effect, *Nat. Commun.* **11**, 5491 (2020).
- [24] S. Longhi, Unraveling the non-Hermitian skin effect in dissipative systems, *Phys. Rev. B* **102**, 201103(R) (2020).
- [25] Y. Yi and Z. Yang, Non-Hermitian Skin Modes Induced by On-Site Dissipations and Chiral Tunneling Effect, *Phys. Rev. Lett.* **125**, 186802 (2020).
- [26] C.-H. Liu, K. Zhang, Z. Yang, and S. Chen, Helical damping and dynamical critical skin effect in open quantum systems, *Phys. Rev. Res.* **2**, 043167 (2020).
- [27] L. Li, C. H. Lee, and J. Gong, Topological Switch for Non-Hermitian Skin Effect in Cold-Atom Systems with Loss, *Phys. Rev. Lett.* **124**, 250402 (2020).
- [28] K. Kawabata, K. Shiozaki, and S. Ryu, Topological Field Theory of Non-Hermitian Systems, *Phys. Rev. Lett.* **126**, 216405 (2021).
- [29] Y. Xiong, Why does bulk boundary correspondence fail in some non-Hermitian topological models, *J. Phys. Commun.* **2**, 035043 (2018).
- [30] F. K. Kunst, E. Edvardsson, J. C. Budich, and E. J. Bergholtz, Biorthogonal Bulk-Boundary Correspondence in Non-Hermitian Systems, *Phys. Rev. Lett.* **121**, 026808 (2018).
- [31] L. Herviou, J. H. Bardarson, and N. Regnault, Defining a bulk-edge correspondence for non-Hermitian Hamiltonians via singular-value decomposition, *Phys. Rev. A* **99**, 052118 (2019).
- [32] D. S. Borgnia, A. J. Kruchkov, and R.-J. Slager, Non-Hermitian Boundary Modes and Topology, *Phys. Rev. Lett.* **124**, 056802 (2020).
- [33] N. Okuma, K. Kawabata, K. Shiozaki, and M. Sato, Topological Origin of Non-Hermitian Skin Effects, *Phys. Rev. Lett.* **124**, 086801 (2020).
- [34] K. Zhang, Z. Yang, and C. Fang, Correspondence between Winding Numbers and Skin Modes in Non-Hermitian Systems, *Phys. Rev. Lett.* **125**, 126402 (2020).
- [35] Y. Ran, Y. Zhang, and A. Vishwanath, One-dimensional topologically protected modes in topological insulators with lattice dislocations, *Nat. Phys.* **5**, 298 (2009).
- [36] V. Juričić, A. Mesaros, R.-J. Slager, and J. Zaanen, Universal Probes of Two-Dimensional Topological Insulators: Dislocation and π Flux, *Phys. Rev. Lett.* **108**, 106403 (2012).
- [37] R.-J. Slager, A. Mesaros, V. Juričić, and J. Zaanen, Interplay between electronic topology and crystal symmetry: Dislocation-line modes in topological band insulators, *Phys. Rev. B* **90**, 241403(R) (2014).
- [38] J. C. Y. Teo and T. L. Hughes, Existence of Majorana-Fermion Bound States on Disclinations and the Classification of Topological Crystalline Superconductors in Two Dimensions, *Phys. Rev. Lett.* **111**, 047006 (2013).
- [39] W. A. Benalcazar, J. C. Y. Teo, and T. L. Hughes, Classification of two-dimensional topological crystalline superconductors and Majorana bound states at disclinations, *Phys. Rev. B* **89**, 224503 (2014).
- [40] F. de Juan, A. Rüegg, and D.-H. Lee, Bulk-defect correspondence in particle-hole symmetric insulators and semimetals, *Phys. Rev. B* **89**, 161117(R) (2014).

- [41] F.-F. Li, H.-X. Wang, Z. Xiong, Q. Lou, P. Chen, R.-X. Wu, Y. Poo, J.-H. Jiang, and S. John, Topological light-trapping on a dislocation, *Nat. Commun.* **9**, 2462 (2018).
- [42] G. van Miert and C. Ortix, Dislocation charges reveal two-dimensional topological crystalline invariants, *Phys. Rev. B* **97**, 201111(R) (2018).
- [43] R. Queiroz, I. C. Fulga, N. Avraham, H. Beidenkopf, and J. Cano, Partial Lattice Defects in Higher-Order Topological Insulators, *Phys. Rev. Lett.* **123**, 266802 (2019).
- [44] M. Geier, I. C. Fulga, and A. Lau, Bulk-boundary-defect correspondence at disclinations in rotation-symmetric topological insulators and superconductors, *SciPost Phys.* **10**, 92 (2021).
- [45] C. W. Peterson, T. Li, W. Jiang, T. L. Hughes, and G. Bahl, Observation of trapped fractional charge and topological states at disclination defects in higher-order topological insulators, [arXiv:2004.11390](https://arxiv.org/abs/2004.11390).
- [46] J. C. Y. Teo and C. L. Kane, Topological defects and gapless modes in insulators and superconductors, *Phys. Rev. B* **82**, 115120 (2010).
- [47] J. C. Teo and T. L. Hughes, Topological defects in symmetry-protected topological phases, *Annu. Rev. Condens. Matter Phys.* **8**, 211 (2017).
- [48] C.-K. Chiu, J. C. Y. Teo, A. P. Schnyder, and S. Ryu, Classification of topological quantum matter with symmetries, *Rev. Mod. Phys.* **88**, 035005 (2016).
- [49] C.-H. Liu and S. Chen, Topological classification of defects in non-Hermitian systems, *Phys. Rev. B* **100**, 144106 (2019).
- [50] A. Panigrahi, R. Moessner, and B. Roy, Non-Hermitian dislocation modes: Stability and melting across exceptional points, [arXiv:2105.05244](https://arxiv.org/abs/2105.05244).
- [51] X.-Q. Sun, P. Zhu, and T. L. Hughes, Geometric Response and Disclination-Induced Skin Effects in Non-Hermitian Systems, *Phys. Rev. Lett.* **127**, 066401 (2021).
- [52] F. Schindler and A. Prem, Dislocation non-Hermitian skin effect, *Phys. Rev. B* **104**, L161106 (2021).
- [53] N. Hatano and D. R. Nelson, Localization Transitions in Non-Hermitian Quantum Mechanics, *Phys. Rev. Lett.* **77**, 570 (1996).
- [54] N. Hatano and D. R. Nelson, Vortex pinning and non-Hermitian quantum mechanics, *Phys. Rev. B* **56**, 8651 (1997).
- [55] All numerical results are obtained using the KWANT code [69].
- [56] C. H. Lee, L. Li, and J. Gong, Hybrid Higher-Order Skin-Topological Modes in Nonreciprocal Systems, *Phys. Rev. Lett.* **123**, 016805 (2019).
- [57] K. Kawabata, M. Sato, and K. Shiozaki, Higher-order non-Hermitian skin effect, *Phys. Rev. B* **102**, 205118 (2020).
- [58] W. P. Su, J. R. Schrieffer, and A. J. Heeger, Solitons in Polyacetylene, *Phys. Rev. Lett.* **42**, 1698 (1979).
- [59] A. Altland and M. R. Zirnbauer, Nonstandard symmetry classes in mesoscopic normal-superconducting hybrid structures, *Phys. Rev. B* **55**, 1142 (1997).
- [60] J. Claes and T. L. Hughes, Disorder driven phase transitions in weak AIII topological insulators, *Phys. Rev. B* **101**, 224201 (2020).
- [61] See Supplemental Material at <http://link.aps.org/supplemental/10.1103/PhysRevB.104.L241402> for derivation of the Chern-Simons topological invariant, and understanding the role of non-topological defects.
- [62] E. I. Blount, Formalisms of band theory, *Solid State Phys.* **13**, 305 (1962).
- [63] J. E. Moore, Y. Ran, and X.-G. Wen, Topological Surface States in Three-Dimensional Magnetic Insulators, *Phys. Rev. Lett.* **101**, 186805 (2008).
- [64] D.-L. Deng, S.-T. Wang, C. Shen, and L.-M. Duan, Hopf insulators and their topologically protected surface states, *Phys. Rev. B* **88**, 201105(R) (2013).
- [65] R. Kennedy, Topological Hopf-Chern insulators and the Hopf superconductor, *Phys. Rev. B* **94**, 035137 (2016).
- [66] C. Liu, F. Vafa, and C. Xu, Symmetry-protected topological Hopf insulator and its generalizations, *Phys. Rev. B* **95**, 161116(R) (2017).
- [67] R. Kennedy and M. R. Zirnbauer, Bott periodicity for Z_2 symmetric ground states of gapped free-fermion systems, *Commun. Math. Phys.* **342**, 909 (2016).
- [68] J. C. Budich and E. J. Bergholtz, Non-Hermitian Topological Sensors, *Phys. Rev. Lett.* **125**, 180403 (2020).
- [69] C. W. Groth, M. Wimmer, A. R. Akhmerov, and X. Waintal, Kwant: A software package for quantum transport, *New J. Phys.* **16**, 063065 (2014).